Research Article

Experimental Study of the Low-Cycle Fatigue in Double-Walled Hollow Pipe Members

Lu Zhaohong [iD],[1] **Zunce Wang** [iD],[1] **Yan Xu** [iD],[1] **Gao Shanshan,**[2] **and Han Lianfu**[1]

[1]*Northeast Petroleum University, Daqing, China*
[2]*Heilongjiang Key Laboratory of Disaster Prevention, Mitigation and Protection Engineering, Daqing, China*

Correspondence should be addressed to Zunce Wang; wangzc@nepu.edu.cn

This paper introduces a double-walled hollow pipe (DWHP) that demonstrates good corrosion resistance and mechanical properties and that can be used in pipeline transportation and structural stress components in marine, freshwater, and corrosive environments. We designed and machined the specimens to meet the bending bearing capacity using a cross section method. We conducted low-cycle loading tests of the specimens to investigate the energy dissipation capacity of the DWHP, the effects of different geometrical parameters, and the concrete-filled strength of the DWHP on energy dissipation capacity. The results show that the failure forms of the specimens are similar. The geometrical characteristics of the specimens, the cohesive function between the concrete and the steel plate, and the strength of the concrete-filled pipe showed a significant influence on the mechanical properties of the specimens. Hysteretic curves are plump and possess a high capacity for energy dissipation. The energy dissipation capacity of the specimen decreases with an increase in the slenderness ratio. The slope of strength degradation decreases with any increase in the strength of the concrete-filled pipe. We optimized the section design of the component by improving the constraint effect coefficient, and we effectively improved its stability by adding stiffeners to the inner side of the outer wall of steel.

1. Introduction

Stainless steel-concrete steel double-walled hollow pipe (DWHP) is a new type of structural component that can be used in engineering for suspended crossover pipes, building structural members, bridges, and offshore platform piles [1]. Because of the high cost of stainless steel materials, they should not be used in engineering applications in large quantities. The outer wall of steel can have a thin stainless steel form. The DWHP section pattern is shown in Figure 1. Steel pipe (e.g., oil and gas pipelines) and the formation of a sandwich component can be used as a new type of combined pipe for pipeline transportation. The cross section of a pipe is a composite structure.

In this study, double-walled hollow-walled concrete-filled steel tubular (CFST) members are considered to have low-cycle fatigue properties.

Scholars have conducted significant research on the mechanical properties of double-walled hollow tube components. Wang et al. [2] and Zhao et al. [3] have studied the

bearing capacity of CFSTs under axial compressive stress and proposed that the confining force between steel pipe and concrete significantly improves the bearing capacity of members. Zhao et al. conducted an axial compression load test on six double-walled hollow-walled CFSTs [4]. The effect of slenderness ratio on the bearing capacity was studied. The bearing capacity of the pipe was found to decrease as the slenderness ratio increased. Elchalakani et al. studied the ductility and failure modes of eight circular concrete-filled double-walled hollow-walled CFST columns under axial compressive load [5]. The experimental results are in close agreement with the standard Load and Resistance Factor Design (LRFD) specification for structural steel buildings [6]. Uy [7] conducted an experimental study on 30 squares of CFST and analyzed the effect of concrete grade and slenderness on the mechanical properties of concrete-filled steel tubes. The results showed that the bearing capacity of CFST columns decreased along with the slenderness ratio and increased along with an increase in concrete grade. Zhao and Grzebieta [8] conducted an experimental study on eight
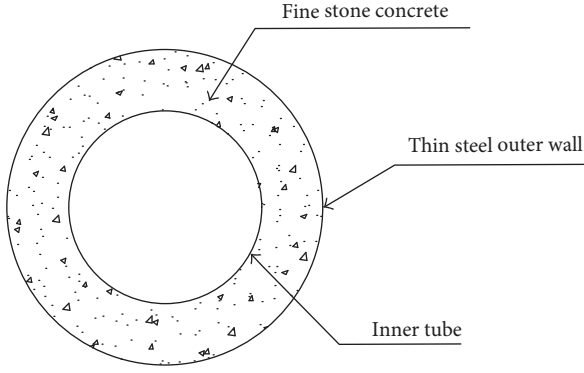
Figure 1: DWHP section pattern.

square concrete hollow stub columns with short columns and five long columns and showed the ratio of outer diameter to thickness to have a significant influence on the performance of hollow-walled CFST columns. Test results have shown that the failure mode of an outer steel wall is similar to that of solid CFST, and the failure mode of an inner steel tube is similar to that of an empty steel tube. Han conducted experiments on a new type of external stainless steel hollow steel tube concrete columns and proposed bearing capacity formula [9]. Huang and Li [10, 11] studied the mechanical properties of hollow-walled CFST under torsional load and steel tube initial stress, respectively, and proposed formulas to guide the engineering design. Lu [12] conducted an experimental study on the fire resistance of six hollow-walled CFST columns. This study examined the combined effect of two layers of steel pipe and a concrete sandwich between composite column specimens, which could be fully exerted under the fire load. Liu [13] conducted a double-walled hollow-tube seismic performance test and finite element analysis. Wang assessed the load-displacement relationship of three kinds of CFSTs and one square concrete-filled double-skin steel tube under reciprocating load [14]. Hong et al. studied the mechanical properties and failure modes of five double-walled hollow CFST short columns that were subjected to compressive, flexural, and shear stresses. The initial stiffness and ultimate load of the double-walled hollow-tube columns decreased as the shear span ratio increased [15].

This research mainly considered the influence of section type, slenderness ratio, and other factors on the bearing capacity and seismic performance of tubes. It did not fully consider the influence of sandwich concrete strength, size effect, or the thin-walled outer layer on the mechanical properties of DWHP components.

On the basis of these research studies, we studied the energy dissipation and antiseismic performance of double-walled hollow CFST members. Through low-cycle loading tests of three specimens, we conducted an analysis of the effects of the geometrical characteristics and filled concrete strength of stainless steel (thin steel outer wall)-concrete steel double-walled hollow-tube specimens on the mechanical properties, including hysteretic capacity, bearing capacity, and stiffness degradation. In conducting this research, we have provided the basis for the research and application of new composite tube members.

2. Test Specimen Design

2.1. Test Specimen Size. To analyze the influence of the thickness of the outer pipe and the strength of the interlayer concrete on the mechanical properties of that pipe, we conducted a comparative analysis in which we kept the inner pipe consistent and changed the parameters of the outer pipe and the strength of the concrete. We selected the wall thickness of the outer pipe according to the sectional stratification method proposed in [1]. We calculated the outer wall thickness t_1, the inner wall thickness t_2, the thickness of the concrete interlayer h, the inner diameter (d), the outer diameter (D), and the bending bearing capacity (M) as follows [1]:

$$h = \frac{D - d}{2} - t_1,$$

$$M = \sum M_k,$$

$$= 2 \sum_{k=0}^{n} \left(\sigma_{s1,k} y_{s1,k} dA_{s1,k} + \sigma_{s2,k} y_{s2,k} dA_{s2,k} + \sigma_{c,k} y_{c,k} a A_{c,k} \right),$$

(1)

where

$$y_{s1,k} = \frac{D}{2} \sin \left(\theta_k - 0.5 \, d\theta \right),$$

$$y_{s2,k} = \frac{d}{2} \sin \left(\theta_k - 0.5 \, d\theta \right),$$

(2)

$$y_{c,k} = \left(\frac{D}{2} - t_1 \right) \sin \left(\theta_k - 0.5 \, d\theta \right),$$

where $\sigma_{s1,k}$ is the outer steel pipe k stratified zone with compressive stress, $\sigma_{s2,k}$ is the inner steel pipe k stratified zone with compressive stress, and $\sigma_{c,k}$ is the k stratified zone concrete compressive stress.

We used the inner tube parameter as the set value to determine the diameter of the outer tube, concrete strength, and maximum bending moment (M). We used a cross section method to calculate the required outer-wall thickness.

According to the requirements of test equipment and the mechanical analysis of test components, we designed a total of three double-walled hollow-walled concrete specimens. The total specimen height was 1520 mm, and the net height was 1200 mm. We used Q235 steel. We filled the specimens with two types of concrete with different degrees of strength: C60 and C40.

The materials and geometrical dimensions of each specimen are given in Table 1.

2.2. Specimen Material Strength. We used the MTS electro hydraulic servo universal testing machine with inner and outer tube steel with unilateral tensile state yield strength of f_{yi} and f_{yo}, ultimate tensile strength of f_{ui} and f_{uo}, elastic modulus E_i, E_o, and other mechanical properties; we determined the cubical compressive strength of the C60 and C40 concrete. We used (3) to calculate the nominal steel

TABLE 1: Geometric parameters of specimens.

Number	Concrete grade	$D_0 \times t_0$ (mm)	$D_i \times t_i$ (mm)	A_{SO} (mm^2)	A_{CE} (mm^2)
DWHP-1	C60	140×2	76×3	867.1	14527
DWHP-2	C60	140×2	76×3	867.1	14527
DWHP-3	C40	110×2	76×3	678.6	8825

TABLE 2: Material performance parameters of specimens.

Number	α_n (%)	ξ	f_{yi} (MPa)	f_{yo} (MPa)	f_{ui} (MPa)	f_{uo} (MPa)	E_i (MPa)	E_o (MPa)	f_{cu} (MPa)
DWHP-1	5.969	0.42	301	288	442	407	1.56E5	1.77E5	63.43
DWHP-2	5.969	0.64	301	288	442	407	1.56E5	1.77E5	42.07
DWHP-3	7.690	1.65	301	288	442	407	1.56E5	1.77E5	42.07

content (α_n) of the pipe and (4) to calculate the steel pipe confinement effect coefficient (ξ).

The material properties and other parameters are given in Table 2.

In Table 2,

$$\alpha_n = \frac{A_{s0}}{A_{CE}}, \tag{3}$$

$$\xi = \alpha_n \frac{f_{y0}}{f_{ck}}, \tag{4}$$

where A_{s0} is the outer tube cross section area and A_{CE} is the outer area surrounded by steel pipe.

3. Test Equipment and Loading System

Considering the second-order (P-Δ) effect of the component, we used a column loading mode. The test device was composed of a concrete floor, a frame to support the vertical load, a beam, and a rolling support. The specimen loading device is shown in Figure 2. We used a DGS-4 computer-controlled electro hydraulic servo-loading system to reciprocate specimen loading. The bottom of the specimen was connected using a fixed steel base, and the top was connected with a crossbeam. The beam was connected to the distribution beam and the horizontal actuator, as shown in Figure 2(a). A vertical load exerted by the hydraulic jack (100 t) above the distribution beam was transmitted to the test piece through the distribution beam and the crossbeam so that the test piece was axially compressed. We used a horizontal actuator (maximum test force of 250 kN, stroke of ±75 mm) on the specimen's horizontal reciprocating load. The rolling support moved freely along the horizontal direction of the track. The rolling support and the crossbeam ensured that the top of the test specimen moved horizontally without twisting or bending.

We applied a vertical hydraulic jack to the specimen to test constant axial force and used the symmetrical displacement method to load the specimen's horizontal reciprocating load.

In the test, we preloaded the vertical load first, and then preloaded the horizontal load step by step. The loading scheme is shown in Figure 3. When the displacement amplitude was less than 6 mm, we loaded it in increments of 1.5 mm. When the amplitude was larger than 6 mm, we loaded it in steps of 6 mm. The load cycle for each stage was completed three times. Damage to the outer wall of the steel tube was the failure criterion for the test. [16].

4. Test Phenomenon and Analysis of Results

4.1. Failure Mode. Figure 4 shows the failure modes of the three test specimens under the action of fatigue load with the same axial compression ratio. The failure occurred toward the end of the specimen, and the damage property was caused by the bending failure. We subjected the specimens to repeated low-cycle loading. When we subjected the test specimen to low cyclic loading, the drum area at the end of the outer steel pipe appeared first, forming a plastic hinge area. Finally, fatigue damage formed in the plastic hinge area at the end of the outer steel pipe, which eventually caused the final damage. During the test, we observed that the outer steel pipe had an obvious tearing failure, which was accompanied by the sound of concrete fracturing. We observed that the concrete fractured after the outer wall was damaged. The bearing capacity of the specimen did not drop abruptly at any point from the loading to the final destruction of the outer wall, and the specimen did not sustain any overall damage, which showed its good ductility and low-cycle fatigue resistance.

4.2. Hysteretic Curve. Figure 5 shows the specimen's moment-curvature (M-φ) hysteretic curve. At the initial stage of test loading, the area covered by the hysteretic curve of the test piece was small. We observed very little residual deformation of the test piece, and rigidity degeneration was not readily visible. The test piece was in an elastic working state. After the initial stage of the test loading, the area of the package gradually increased along with an increase in the number of loading cycles and the control displacement. The hysteretic curve tilted toward the displacement axis. The rigidity of the specimen began to decrease and entered the plastic working state. When we applied the maximum load, the specimen-bearing capacity and energy consumption began to decline gently.

Comparing the M-φ hysteretic curves of the specimens, we found the following: (1) The hysteresis curve of DWHP-1 was fuller, and the peak load capacity was greater than
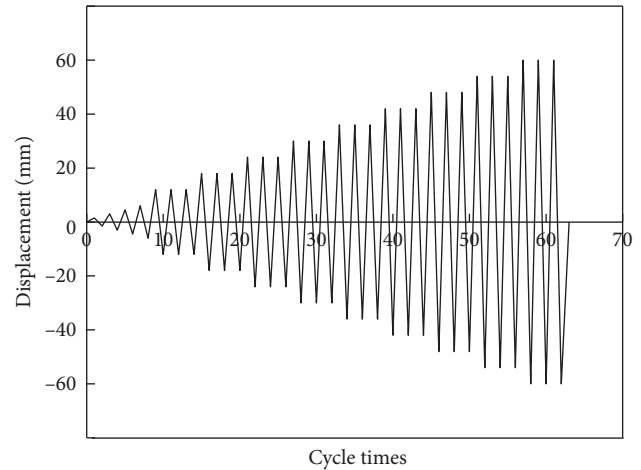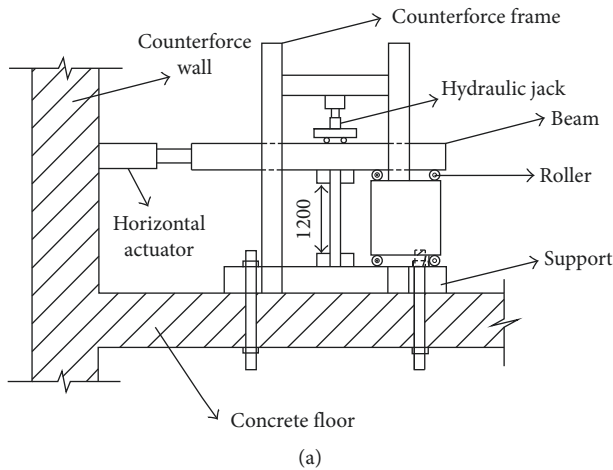
(a)

(b)

Figure 2: Loading device for specimen. (a) Sketch of sample loading device and (b) sample loading device spot map.

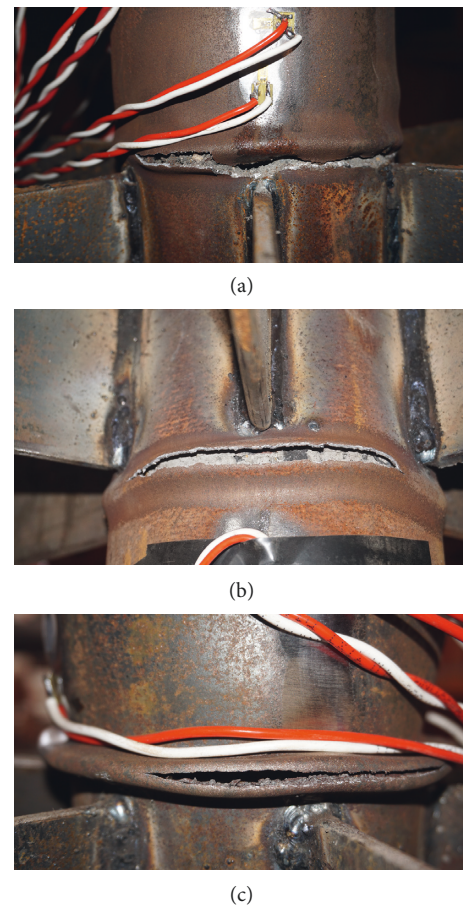Figure 3: Sketch of loading scheme.

(a)

(b)

(c)

Figure 4: Failure modes of specimens. (a) Lower-end tearing of DWHP-1, (b) upper-end tearing of DWHP-2, and (c) lower-end tearing of DWHP-3.

DWHP-2 and DWHP-3 specimens for the same geometric size, steel strength, and axial compression ratio. In this way, ductility and energy dissipation capacity of the specimens can be improved by appropriately increasing the strength of the concrete. (2) The specimen of DWHP-3 had a smaller section size and a lower strength level of concrete. The hysteretic curve was full, without a significant pinch phenomenon and showed good hysteretic performance. The analysis showed that although the cross section dimension of the DWHP-3 specimen was the smallest, the restraining effect coefficient ξ of this specimen was the largest, which
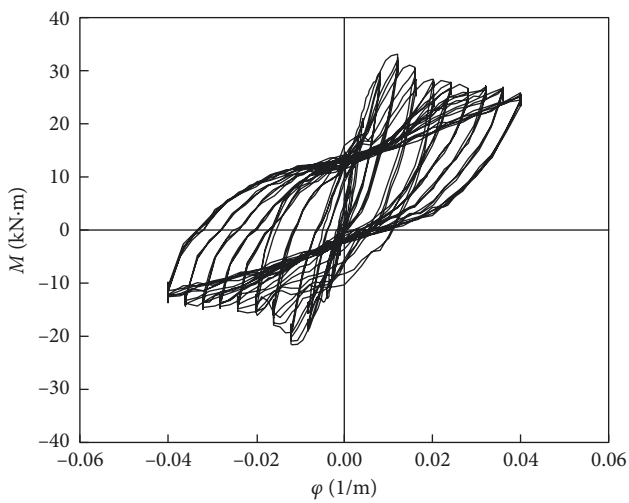
was 2.5 times that of specimen DWHP-2 and 3.9 times that of specimen DWHP-1. Improving the component confinement factor can reduce the section size or the strength grade of the concrete, which is the purpose of optimizing the design of the structure.
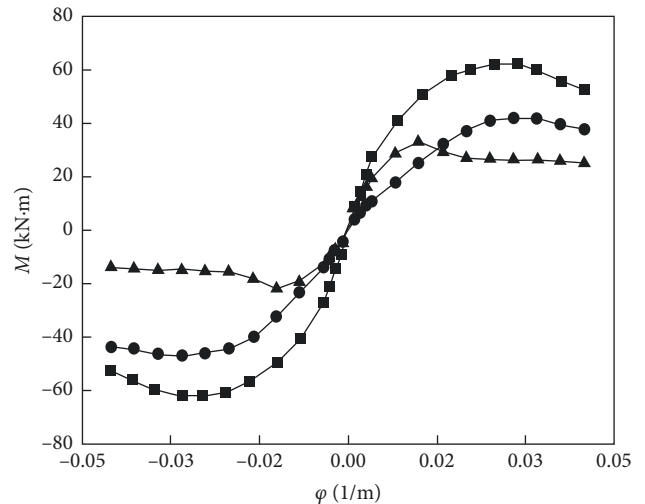
(a)

(b)

(c)
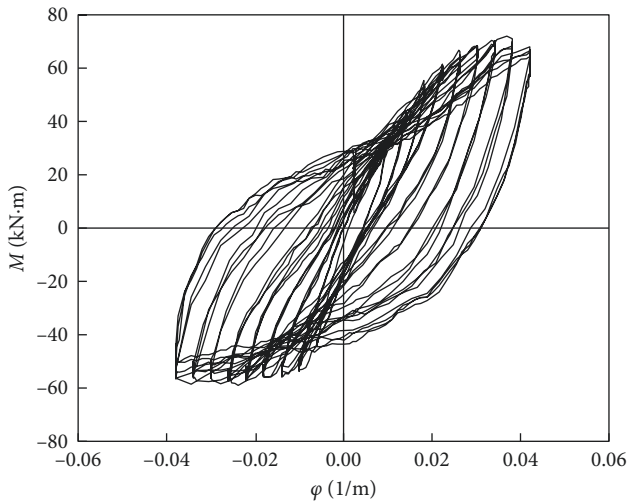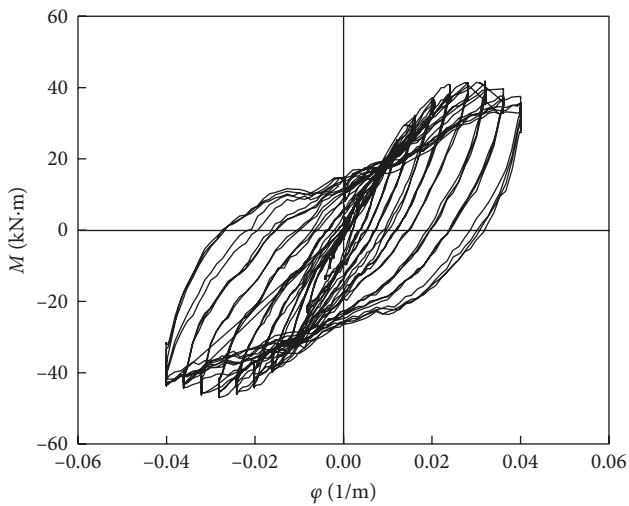
FIGURE 5: M-φ hysteretic loops of specimens. (a) Specimen DWHP-1, (b) specimen DWHP-2, and (c) specimen DWHP-3.

- DSTM-1
- DSTM-2
- DSTM-3

FIGURE 6: M-φ skeleton loops of specimens.

4.3. Skeleton Curve. We obtained the P-Δ skeleton curve of the specimen by first connecting the peak load points of the tested M-φ hysteretic curve to each target displacement [17]. The results are shown in Figure 6. Under low-cycle loading, the specimens underwent four working stages: elasticity, yield, peak, and damage. At the initial stage of specimen loading, the skeleton curve developed linearly. When the curve was loaded with an obvious inflection point, the specimen began to yield, and the stiffness began to degrade. As the control displacement increased, the stiffness of the specimen degenerated further. When the peak point of the skeleton curve was reached, the degradation of the bearing capacity of the specimen changed more smoothly. The results showed that the degradation rate of DWHP-2 was greater than that of DWHP-1 and smaller than that of DWHP-3. DWHP-3 showed significant degradation at the target displacement of ±20.

We analyzed the phenomenon by which the double-wall sandwich-filled concrete under the constraint of the double steel pipe in a three-dimensional compression could improve the strength of filled concrete, allow the concrete to be filled with steel to provide lateral support, and protect the thin steel wall from local instability. Under these working conditions, the specimen showed good overall plasticity and ductility. The outer side of the steel pipe had a thin steel layer, however, and its stability was greatly influenced by the bond between the concrete and the steel plate, and the strength of the concrete had a great influence on the ductility of the components. Within a certain range, the strength of the concrete could effectively increase the specimen ductility and improve fatigue resistance. The analysis showed that the reinforcement of the steel plate and the concrete could be strengthened by adding reinforcing ribs inside the outer wall, which effectively improved the local stability of the
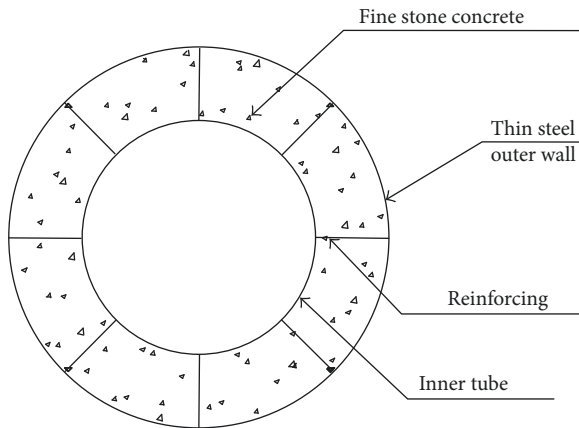
FIGURE 7: Section type of the stiffener pipe.

TABLE 3: Energy dissipation of each cycle of specimen displacement.

Displacement	Hysteretic energy consumption (kN·mm)		
	DWHP-1	DWHP-2	DWHP-3
±6	48.49	45.29	32.96
±12	244.19	131.69	197.74
±18	444.58	201.09	332.2
±24	792.99	407.09	559.95
±30	1160.9	649.53	833.49
±36	1723.7	992.97	788.83
±42	2249.4	1279.5	754.16
±48	2921.8	1817.2	929.64
±54	3613.1	2305.3	1102.5
±60	4426.5	2659.4	1258.5

component. The addition of an outer-wall stiffener is shown in Figure 7.

4.4. Hysteretic Energy Consumption. We used the plastic hysteretic energy of the component to evaluate the seismic behavior of the structure. The numerical value was proportional to the seismic performance of the structure. The better the seismic performance of the buildings, the greater the plastic hysteretic energy value would be. In this experiment, the sum of the energy absorbed by the specimen was expressed as the area of the closed hysteretic loop formed after one week of the test specimen's circulation [17, 18]. We calculated the total hysteretic energy of the specimen according to the following equation:

$$W_p = \sum_{i=1}^{n} W_i, \qquad (5)$$

where n is the ith cycle load times and W_i is i-hysteretic loop energy value.

The size of the area enclosed by the hysteretic ring reflects the pros and cons of the seismic performance of the structure to a certain extent. The energy dissipation values of the top of the member at each stage of the displacement cycle are given in Table 3.

To facilitate a comparative analysis, we assessed the axial loading-displacement curve fitted to each ring hysteretic loop, using the size of that area to indicate the hysteretic energy value. The sum of the energy dissipation values of the specimen in the displacement cycle at various stages is shown in Figure 8.

The hysteretic energy dissipation diagrams of DWHP-2 and DWHP-1 show that the other conditions are the same. When the concrete strength changed from 42.07 MPa to 63.43 MPa, the hysteretic energy of the specimen was controlled and changed from 2659.4 kN·mm to 4426.5 kN·mm, an increase of 1.66 times.

Compared with DWHP-3 and DWHP-2, the hysteretic energy loss of DWHP-3 was greater than that of DWHP-2 before the initial displacement and before the displacement of the 30 mm hysteretic energy value. When the control displacement was greater than 30 mm, the DWHP-3
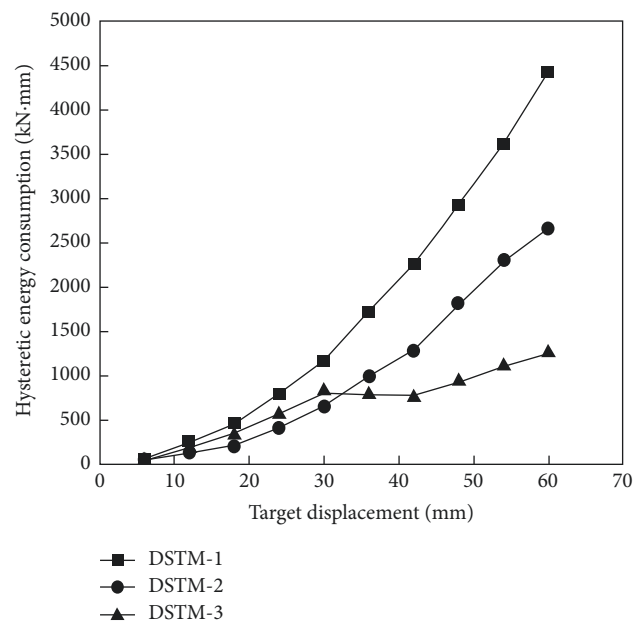

FIGURE 8: Hysteretic energy of specimens.

hysteretic energy value had a sudden downward trend and gradually fell below the DWHP-2 hysteretic energy value. When the control displacement reached ±42 mm, the bearing capacity of DWHP-3 decreased to about 80% of the peak load. The energy dissipation value of DWHP-3 began to increase as the target displacement increased, but the range of increase was obviously smaller than that of DWHP-2. An analysis of these test results suggested that the high-strength concrete made up for the brittleness defects of the material under the restraint of the double-layer steel pipe inside and outside greatly improved the energy-absorbing and damping capacity of the component. Because of the thin-walled steel pipe, under the condition of the same concrete strength, the size of the component had a greater impact on energy dissipation capacity. When the strength of the member reached about 80% of the yield load, the energy dissipation capacity of the ASTM-3 small section member had a downward trend when the displacement of the target was 30 mm.
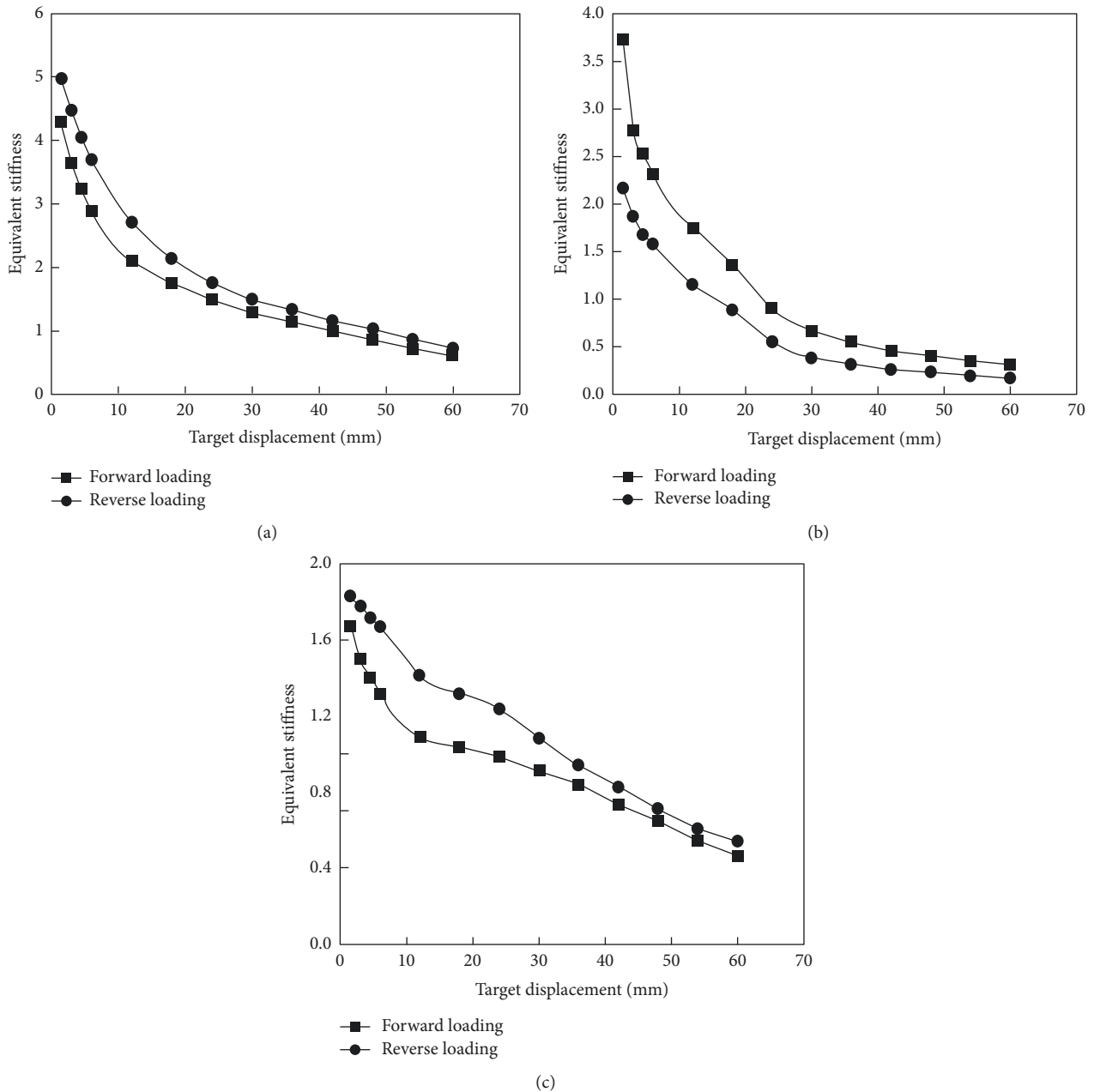
(a)

(b)

(c)

FIGURE 9: Degeneration rigidity loops of specimens. (a) Specimen DWHP-1, (b) specimen DWHP-2, and (c) specimen DWHP-3.

4.5. Stiffness Degradation.

We used the equivalent stiffness to show the stiffness decay of the specimen under low-cycle loading. The stiffness of each specimen was the ratio of the corresponding load value to the target displacement value when the target displacement was reached for the first time. Equivalent stiffness of the specimen expression [19] is shown in the following:

$$K = \frac{P}{\Delta}. \tag{6}$$

Equivalent stiffness decay curve when the specimen is loaded is shown in Figure 9.

As shown in Figure 10, the stiffness degeneration trend of each specimen was similar; all specimens experienced

a degeneration process that changed from fast to slow. In the initial stage of loading, the specimen was in a flexible working condition and had the most rigidity. With the gradual increase of displacement of the experimental target, concrete cracks and continuous development of specimens increased until plastic deformation gradually occurred. When the relative slip between the inner and outer steel pipes and the filled concrete occurred, the restraint effect of the steel pipe on the core concrete began to weaken. The initial stiffness of specimens DWHP-1 and DWHP-2 with the same cross section size and different concrete strength was about 4.5 and 3.0, respectively. However, the degeneracy curves were basically the same and their stiffness degenerated similarly. The initial stiffness of DWHP-2 and
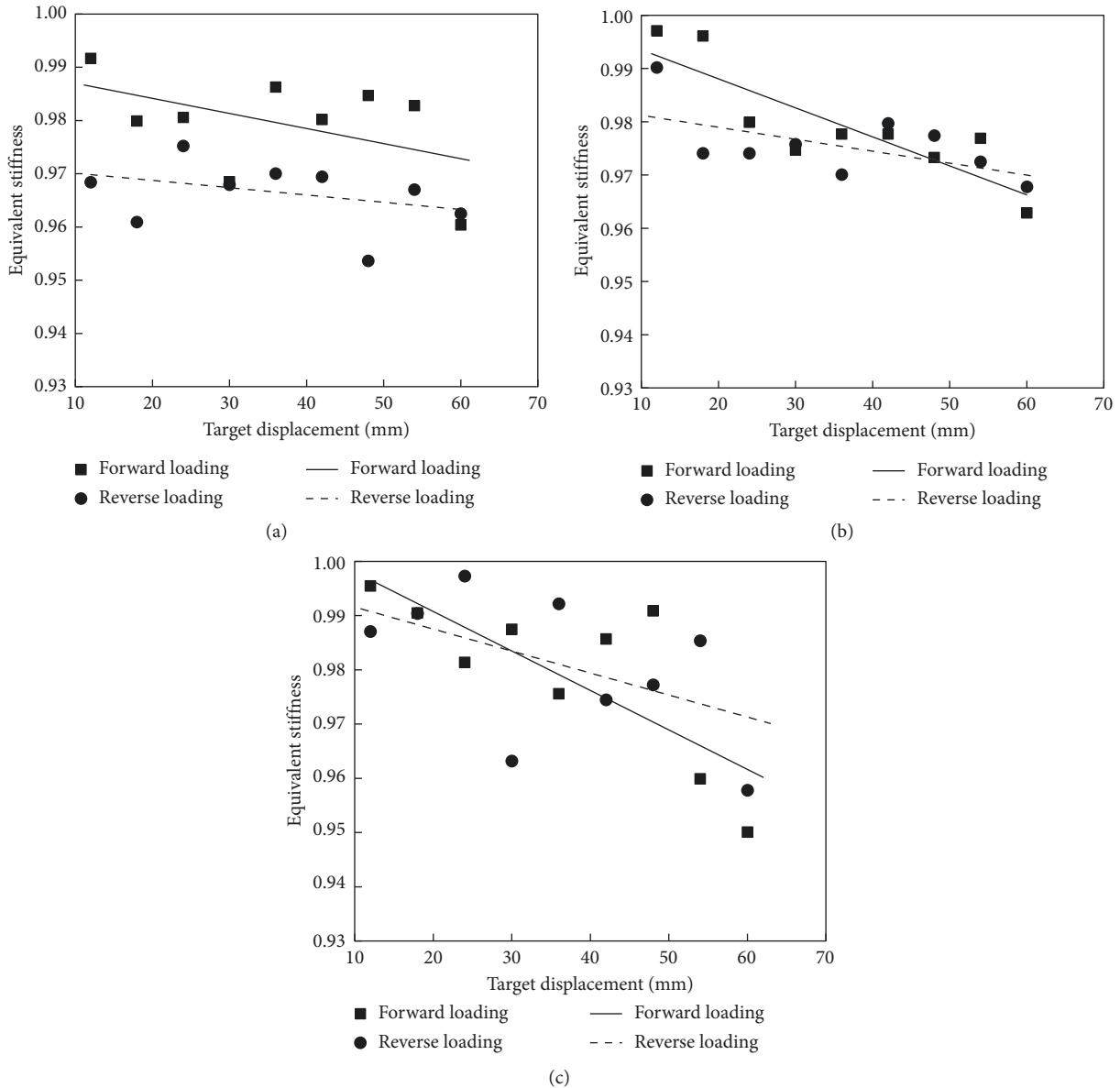
FIGURE 10: Degeneration loading loops of specimens. (a) Specimen DWHP-1, (b) specimen DWHP-2, and (c) specimen DWHP-3.

DWHP-3 with the same concrete strength and different cross section dimensions was about 3.0 and 1.7, respectively. The linear regression curves showed that the degeneracy rate of DWHP-3 was larger than that of DWHP-2.

According to the analysis of the test phenomenon, the initial elastic stiffness of the specimen was closely related to the concrete strength, whereas the stiffness degradation rate was less affected by the concrete strength under the reciprocating loading. The cross section dimension had a significant effect on the initial elastic stiffness and the rate of stiffness degradation. The larger the initial cross section stiffness, the lower the rate of stiffness degradation would be.

4.6. Intensity Degradation. The specimen's bearing capacity was largest when the specimen reached the target displacement for the first time. The calculated value of the

degradation of bearing capacity was the load value Pi when the specimen reached the displacement at the ith time and was divided by the load value $P1$ when the specimen reached displacement the first time. We compared the second load value under each control displacement with the first load ratio of $P2/P1$ to analyze the bearing capacity of the specimen decay. The bearing capacity degradation curve for each specimen is shown in Figure 10.

The results show that under the action of repeated low-cycle loading, the internal damage of the specimen developed, and the bearing capacity gradually decayed. The bearing capacity decay rule of each specimen was similar to the decay of bearing capacity of three specimens, and there was no significant attenuation of bearing capacity during the entire experiment. The loading rate of specimen DWHP-1 decayed slowly, and the slope of strength degradation was the smallest. The slope of bearing capacity degradation of

specimen DWHP-2 was similar to that of specimen DWHP-3. As shown, under cyclic loading, the slope of degradation was greatly affected by the strength of concrete. The higher the strength was, the smaller the slope of degradation was and the smaller the effect of size effect was.

5. Conclusion

According to the quasistatic test method, we conducted a low-cycle fatigue test of three double-walled hollow CFST specimens with different geometrical characteristics and different filled concrete strengths. The main conclusions are as follows:

(1) We calculated the bending design of DWHP using the cross section method. Through a low-cycle loading test, the results showed that the strength grade of the C60 sandwich concrete, under the same geometrical size, steel strength, and axial compression ratio, had better ductility and energy dissipation capacity than that of the C40 concrete specimen. The ductility and energy dissipation capacity of the specimens could be improved by strengthening the concrete. Analysis showed that although the cross section dimension of DWHP-3 specimen was the smallest, the restraining effect coefficient ξ of this specimen was the largest, which was 2.5 times that of specimen DWHP-2 and 3.9 times that of specimen DWHP-1. The DWHP-3 specimen still had good ductility and energy dissipation capacity by improving the confinement factor to appropriately reduce the section size or strength grade of the concrete to optimize the design of the structural section.

(2) The combination of DWHP concrete sandwich members, concrete, and steel worked together to ensure that the mechanical properties provided the specimens with higher strength and ductility. But the outer side of the steel pipe was a thin steel layer, and the bond between the concrete and the steel plate had a significant influence on the stability of the concrete. Because of the cohesive force, the strength of the concrete did not have an obvious influence on the local instability of the components. The analysis showed that addition of reinforcing ribs on the inner side of the outer wall of the steel pipe could improve the adhesion of the thin steel plate to the concrete, which could effectively improve the local stability of the specimens.

(3) The composite cross section of the outer steel pipe for the thin steel layer, under the conditions of the same concrete strength, showed that the size of the component had a greater impact on energy dissipation capacity. When the strength of the specimens reached about 80% of the yield load, the energy dissipation capacity of the small section specimens had a downward trend when the displacement of the target was 30 mm. The main cause of the smaller yield displacement was the smaller geometrical dimension of the specimen.

(4) Under cyclic loading of DWHP, the strength degradation slope of the C60 sandwich concrete was obviously lower than that of the C40 concrete specimen. The slope of the strength degradation of the specimens decreased with an increase in the strength of the filled concrete within a certain range, but the strength degradation slope was less affected by geometric characteristics.

Conflicts of Interest

The authors declare that they have no conflicts of interest.

Acknowledgments

References

[1] L. Zhaohong, Y. Liang, G. M. Zhang et al., "Calculation of the flexural capacity of double-skin-tubular members by section stratification method," *Journal of Hebei University of Engineering*, vol. 4, pp. 11–14, 2015.

[2] Z. Wang, W. Zhang, S. Chi et al., "Flexural behavior of composite concrete-filled square thin-walled steel tubular specimens," *Journal of Building Structures*, vol. 38, no. 7, pp. 78–84, 2017.

[3] J. Zhao, H. Guo, and X. Wei, "Research on bearing capacity of concrete filled double skin steel tubes column," *Journal of Architecture and Civil Engineering*, vol. 22, no. 1, pp. 50–54, 2005.

[4] X. L. Zhao, R. H. Grzebieta, and M. Elchalakani, "Tests of concrete-filled double skin circular hollow sections," in *Proceedings of the First International Conference on Steel and Composite Structures*, pp. 283–290, Pusan, Korea, June 2001.

[5] M. Elchalakani, X. L. Zhao, and R. Grzebieta, "Tests on concrete filled double-skin (CHS outer and SHS inner) composite short columns under axial compression," *Thin-Walled Structures*, vol. 40, no. 5, pp. 1–28, 2002.

[6] Z. Raochun and Z. Xuhong, *The Principle of Steel Structure Design*, Higher Education Press, Beijing, China, 2013.

[7] B. Uy, "Strength of concrete filled steel box columns incorporating local buckling," *Journal of Structural Engineering*, vol. 126, no. 3, pp. 341–352, 2000.

[8] X. L. Zhao and R. Grzebieta, "Strength and ductility of concrete filled double-skin (SHS inner and SHS outer) tubes," *Thin-Walled Structures*, vol. 40, no. 2, pp. 199–213, 2002.

[9] L. H. Han, Q. X. Ren, and W. Li, "Tests on stub stainless steel-concrete-carbon steel double-skin tubular (DST) columns," *Journal of Constructional Steel Research*, vol. 67, no. 3, pp. 437–452, 2011.

[10] H. Huang, L. H. Han, and X. L. Zhao, "Investigation on concrete filled double skin steel tubes columns under pure torsion," *Journal of Constructional Steel Research*, vol. 90, no. 1, pp. 221–234, 2013.

[11] W. Li, L. H. Han, and X. L. Zhao, "Axial strength of concrete-filled double skin steel tubular columns with preload on steel tubes," *Thin-Walled Structures*, vol. 56, no. 1, pp. 9–20, 2012.

[12] H. Lu, L. H. Han, and X. L. Zhao, "Fire performance of self-consolidating concrete filled double skin steel tubular

columns experiments," *Fire Safety Journal*, vol. 45, no. 2, pp. 106–115, 2010.

[13] Y. Liu, *Finite Element Analysis on Axial Compression and Seismic Behaviors of Multibarrel Tube-Confined Concrete*, Chang'an University, Xi'an, China, 2015.

[14] N. Wang, *Experimental Research and Numerical Simulation of Concrete-Filled Double Skin Steel Tubes-Columns*, Hebei University of Engineering, Hebei, China, 2013.

[15] H. Hong, S. Wei, C. Meng Cheng et al., "Experimental study on concrete-filled double-skin circular steel tubes under combined loadings," *Journal of Building Structures*, vol. 9, pp. 53–59, 2015.

[16] T. Zirakian and J. Zhang, "Buckling and yielding behavior of unstiffened slender, moderate, and stocky low yield point steel plates," *Thin-Walled Structures*, vol. 88, pp. 105–118, 2015.

[17] B. Zhu, *Structural Seismic Test*, Seismological Press, Beijing, China, 1989.

[18] W. Zhang and W. Zhao, "On the issues of life cycle fatigue damage for the columns of concrete-filled steel tubular," in *Proceedings of the 17th National Conference on Structure Engineering*, pp. 684–687, Huazhong University of Science and Technology, Wuhan, Hubei, China, 2008.

[19] J. Zhou and S. Chen, *Experimental Study and Evaluation Method of Mechanical behavior of High Strength Reinforced-Concrete Structure*, Science Press, Beijing, China, 2015.